Available online at www.sciencedirect.com

SciVerse ScienceDirect

Geochimica et Cosmochimica Acta 80 (2012) 1–13

Geochimica et Cosmochimica Acta

www.elsevier.com/locate/gca

In situ nanoscale observations of the dissolution of $\{10\bar{1}4\}$ dolomite cleavage surfaces

Maja Urosevic [a], Carlos Rodriguez-Navarro [a], Christine V. Putnis [b], Carolina Cardell [a], Andrew Putnis [b], Encarnación Ruiz-Agudo [a,b,*]

[a] Department of Mineralogy and Petrology, University of Granada, Fuentenueva s/n, Granada, Spain
[b] Institut für Mineralogie, Universität Münster, Corrensstrasse 24, 48149, Münster, Germany

Received 19 April 2011; accepted in revised form 16 November 2011

Abstract

Knowledge of the kinetics and mechanisms of carbonate dissolution is essential, for instance, to determine the contribution of carbonate-fluid reactions to the global carbon cycle and CO_2 sequestration strategies, as well as to design new methods that mitigate the effects of weathering processes on carbonate stones. There is a significant lack of understanding of the molecular-scale reaction mechanisms of dolomite ($CaMg(CO_3)_2$), particularly in comparison to other common carbonates such as calcite ($CaCO_3$). Here we present a systematic in situ Atomic Force Microscopy (AFM) study of dolomite dissolution in the pH range 3–10 aimed at improving our understanding of the nanoscale processes governing dolomite–fluid interactions. The results of this study indicate that the overall dolomite dissolution rate is controlled by the removal of dolomite layers by spreading and coalescence of shallow etch pits, nucleated at point defects and/or in defect-free areas. Our results also suggest that at all pH (and particularly at pH <5) and under conditions of relatively slow solution flow, dolomite dissolves via a dissolution–precipitation reaction with the formation of an Mg-rich surface precipitate. As a consequence, the effluent solution shows Ca/Mg ratios >1. This explains why in the past the dolomite dissolution was considered to be "incongruent". In situ, direct observations of the reacting mineral surfaces are important to unambiguously ascertain the kinetics and mechanism of mineral dissolution. In fact, direct observations allow quantification of the kinetics of the process from the measurement of etch pit spreading rates, which are unaffected by the formation of a secondary precipitate whose existence has been neglected in the past.

1. INTRODUCTION

Dissolution of carbonate minerals is one of the main chemical reactions occurring at shallow levels in the crust of the Earth and has a paramount importance for a wide range of geological and biological processes. In particular, carbonate dissolution plays a key role in a large spectrum of scenarios such as landscape modeling and carbonate aquifer development (i.e. Karst geomorphology, e.g. Ford and Williams, 2007), the chemistry of marine waters and global carbon cycle (Oelkers and Schott, 2005; Millero, 2007), in engineering science (e.g. carbonate dissolution enhances permeability and increases oil reservoir productivity, Lund et al., 1973), cultural heritage and building stone preservation (Bell, 1993; Charola and Ware, 2002; Cardell Fernández et al., 2002; Hoke and Turcotte, 2004), and biomineralization (Mann, 2001). Calcite ($CaCO_3$), and to a lesser extent dolomite ($CaMg(CO_3)_2$), are the major carbonate minerals in sedimentary rocks. The dissolution of calcite has been thoroughly investigated over a range of conditions and solution compositions (see Morse et al. (2007) for a comprehensive review). In contrast, dolomite

* Corresponding author at: Department of Mineralogy and Petrology, University of Granada, Fuentenueva s/n, Granada, Spain.
E-mail addresses: maja@ugr.es (M. Urosevic), carlosrn@ugr.es (C. Rodriguez-Navarro), putnisc@uni-muenster.de (C.V. Putnis), cardell@ugr.es (C. Cardell), putnis@uni-muenster.de (A. Putnis), encaruiz@ugr.es, eruiz_01@uni-muenster.de (E. Ruiz-Agudo).

0016-7037/$ - see front matter © 2011 Elsevier Ltd. All rights reserved.
doi:10.1016/j.gca.2011.11.036

dissolution studies have been traditionally hampered by its low reaction rates compared to calcite and the poorly constrained relationship between cation ordering and reactivity in dolomite (e.g. Morse and Arvidson, 2002; Lüttge et al., 2003).

Dolomite dissolution rate is a complex function of saturation state, pH, temperature, ionic strength, total dissolved carbonate, aqueous calcium and magnesium activities, organic and inorganic ligand concentration and hydrodynamic conditions (Busenberg and Plummer, 1982; Herman and White, 1985; Chou et al., 1989; Orton and Unwin, 1993; Pokrovsky and Schott, 2001; Pokrovsky et al., 2005; Gautelier et al. 2007). Most of these relationships have been derived experimentally by monitoring the evolution of the composition of the bulk solution using macroscopic flow-through or batch reaction devices. Direct observations of mineral growth and dissolution by real-time nanometer-resolution imaging techniques such as in situ Atomic Force Microscopy (AFM), Lateral Force Microscopy (LFM) and Vertical Scanning Interferometry (VSI) have proven to be critical for determining the mechanism and kinetics of mineral dissolution, as they facilitate a precise and representative analysis of mineral–water interactions (see for example Lüttge et al., 2003; Higgins and Hu, 2005; Ruiz-Agudo et al., 2009). Despite the existence of several macroscopic studies dealing with dolomite dissolution, very little work has been done towards the understanding of the reactivity of dolomite interfaces at the molecular scale (Lüttge et al., 2003; Higgins and Hu, 2005; Hu et al., 2005; ; Fenter et al., 2007; Higgins et al., 2007; Kaczmarek and Sibley, 2007; Ruiz-Agudo et al., 2011). Although these nanoscale resolution studies have provided new insights into the kinetics and mechanisms of dolomite dissolution there is still a significant lack of understanding of the molecular-scale reaction mechanisms of dolomite, particularly in comparison to other common carbonates such as calcite (Fenter et al., 2007).

All previous nanoscale studies of dolomite dissolution rates have been conducted at fixed pH conditions and, to date, there is not a systematic study of the dependence of dissolution rates on pH as in the case of macroscopic flow-through or batch reaction experiments (e.g. Chou et al. 1989; Gautelier et al., 1999; Pokrovsky et al., 1999; Pokrovsky and Schott, 2001). Moreover, there is a significant scattering on the published data of macroscopic dolomite dissolution rates as a function of pH, possibly due to the fact that these studies are performed under different hydrodynamic conditions, ionic strength and/or pco_2. Nevertheless, all these works agree that the dolomite dissolution reaction is complex compared to other common carbonates such as calcite, aragonite or magnesite, as reflected for example in the determined fractional-order dependence of the dolomite dissolution rate on H^+ activity (at low pH and in the absence of CO_2) (c.f. Busenberg and Plummer, 1982; Chou et al., 1989; Orton and Unwin, 1993).

The aim of this paper is to present a systematic in situ AFM study of dolomite dissolution in the pH range 3–10 in order to improve our knowledge of the nanoscale processes governing dolomite–fluid interactions. Experiments were carried out far from equilibrium (no calcium, magnesium, bicarbonate or carbonate in the inlet solutions) and at low ionic strength. A better understanding of the kinetics and mechanisms of dolomite dissolution at different pH is essential, for instance, to determine the contribution of dolomite–fluid reactions to the global carbon cycle and CO_2 sequestration strategies (c.f. Oelkers and Schott, 2005; Gautelier et al., 2007), as well as to design new methods that mitigate the effects of acid rain on carbonate stone.

2. METHODOLOGY

2.1. Atomic Force Microscopy (AFM)

High purity, optical grade dolomite crystals from Eugui, Navarra (Spain) were cleaved with a knife blade to obtain mm-size (ca. $3 \times 3 \times 1$ mm) fragments. Crystallinity of the sample was checked previously by powder X-ray diffraction (XRD) that showed the presence of strong cation ordering (or superstructure) reflections (i.e., those with indexes $(h0l)$ and $(0kl)$, with odd-numbered l, such as (1 0 1), (0 1 5), and (1 0 7); Lippman, 1973) confirming its crystalline perfection. Due to its chemical purity and crystalline perfection dolomite single crystals from this locality in Navarra have been used in several studies of dolomite dissolution (e.g., Busenberg and Plummer, 1982; Orton and Unwin, 1993; Lüttge et al., 2003). AFM in situ dissolution experiments were carried out by passing solutions of fixed pH over dolomite $\{10\bar{1}4\}$ cleavage surfaces. Solutions used in the experiments were prepared using double-deionized water (resistivity $>18\ m\Omega\ cm^{-1}$) and the solution pH was adjusted from 3 to 10 using HCl or NaOH. Each solution was prepared immediately before the experiment to avoid equilibration with the ambient air, especially at higher pH values. Therefore, the amount of carbonate and bicarbonate ions in solution is considered to be negligible. The absence of calcium and magnesium in the input solutions ensured constant far-from-equilibrium conditions with respect to dolomite. In situ observations and measurements were performed using an AFM equipped with a fluid cell of a Digital Instruments Nanoscope III Multimode AFM working in contact mode under ambient conditions ($T = 20$ °C). The solutions flowed continuously for 30 min at ca. 100 mL h^{-1} from a syringe coupled to an O-ring-sealed fluid cell containing the sample crystal. The scanned areas were typically 9 $(3 \times 3)\ \mu m^2$. AFM images were collected using Si_3N_4 tips (Veeco Instruments, tip model NP-S20) and analyzed with the Nanoscope software (Version 5.12b48). Measurements of step retreat velocity (or etch pit spreading rate, v_{sum}) were made from sequential images scanned in the same direction. The retreat velocity given by $v_{sum} = (v_+ + v_-)$, where v_+ and v_- represent the retreat velocities of + and − steps, respectively (see Paquette and Reeder (1995) for a comprehensive description of the morphology and nomenclature of rhombohedral carbonate etch pits). v_{sum} values were calculated by measuring the length increase per unit time between opposite parallel steps in sequential images. Overall dissolution rates, R_{AFM} (in mol $cm^{-2}\ s^{-1}$), were calculated as follows: if there are N_{pit} etch pits per square centimeter of surface,

then for a shallow rhombohedral etch pit, the volume loss (V) after the time between two sequential images t_2-t_1, can be approximated by

$$\Delta V = (w_2 \cdot u_2 - w_1 \cdot u_1) \cdot h \quad (1)$$

where w, u and h are the etch pit width, length and depth, respectively, in sequential images after that time duration, t_2-t_1. Therefore, the overall dissolution rate (mol cm^{-2} s^{-1}) can be calculated as

$$R_{\mathrm{AFM}} = \frac{\Delta V \cdot N_{\mathrm{pit}}}{V_{\mathrm{dol}} \cdot (t_2 - t_1)} \quad (2)$$

where V_{dol} is the molar volume of dolomite (64.34 cm^3 mol^{-1}). N_{pit} used in the calculation of the overall dissolution rates is the average observed for each experiment.

Additionally, after flowing through the fluid cell 10 mL aliquots of effluent solution were collected for calcium and magnesium analysis by inductively coupled plasma optical emission spectrometry, ICP-OES (Varian Vista proaxial). In flow through experiments performed in AFM, the use of geometric surface area as reactive area contributes to significant error in macroscopic rate determinations, leading to an overestimation of macroscopic dissolution rates (Duckworth and Martin, 2004; Ruiz-Agudo et al., 2010, 2011). The very low amount of calcium and magnesium in the outlet solution (a few ppm) precludes obtaining reliable concentration values (Arvidson et al., 2006). Nevertheless, here we present a few selected measured values of macroscopic dissolution rates only for comparison purposes. Macroscopic dissolution rates of dolomite, R_{mac} (mol cm^{-2} s^{-1}) were calculated as follows:

$$R_{\mathrm{mac}} = \frac{\mathrm{Ca_T} Q}{A} \quad (3)$$

where $\mathrm{Ca_T}$ is the total calcium in the effluent solution (mol L^{-1}), Q is the solution flow rate (L s^{-1}) and A is the geometric surface area of dolomite exposed to the solution (cm^2). As it will be discussed thoroughly below, dolomite is known to dissolve "incongruently", as reflected in the Ca/Mg ratios higher than one measured in the outflow. For this reason, calculation of dissolution rates using measured Mg fluxes was discarded.

2.2. Analysis of surface precipitates

AFM flow-through experiments were reproduced in flow-through Teflon reactors (inner volume 4 mL) and after flowing a HCl solution (pH 2.84) over the crystal for 30 min (flow rate of ca. 100 mL h^{-1}) the crystals were analyzed by X-ray diffraction (XRD), using a Philips PW XPERT-PRO diffractometer (Department of Mineralogy and Petrology, University of Granada). In order to maximize the signal from the thin surface layer of the precipitate and minimize the penetration depth of the X-rays into the dolomite substrate, data were obtained in grazing incident angle mode (GIAXRD), by carrying out 2θ scans at a fixed small incident angle of the X-ray beam on the substrate surface. Analysis conditions were: radiation Cu Kα (λ: 1.5405 Å), 45 kV voltage, 40 mA current intensity, and goniometer speed of 0.01° 2θ/s using Si-detector X'Celerator. The grazing angle (ω) was 2° and the investigated area between 5° and 60° 2θ. The study of diffractograms was performed using the computer program X'Pert Plus V.1.0 (1999, PANalytical). The crystals were also analyzed by X-ray photoelectron spectroscopy (XPS). We used a Physical Electronic PHI 5701 spectrometer equipped with a multichannel hemispherical electroanalyzer. Non-monochromatic Mg Kα X-ray radiation (300 W, 15 kV, 1253.6 eV) was used as the excitation source. The spectrometer energy scale was calibrated using Cu 2p3/2, Ag 3d5/2, and Au 4f7/2 photoelectron lines at 932.7, 368.3 and 84.0 eV, respectively. The binding energy of photoelectron peaks was referenced to C1s core level for adventitious carbon at 284.8 eV. High resolution spectra were recorded at a given take-off angle of 45° by a concentric hemispherical analyzer operating in the constant pass energy mode at 29.35 eV and using a 400 μm diameter aperture. The residual pressure in the analysis chamber was maintained below 1.33×10^{-7} Pa during spectra acquisition. The PHI ACCESS ESCA-V8.0C software package was used for acquisition and data analysis. Recorded spectra were fitted using Gauss–Lorentz curves in order to accurately determine the binding energy of the different element core levels. After a Shirley-type background subtraction, atomic concentration percentages of the dolomite elements were determined from high-resolution spectra and the corresponding area sensitive factor for every photoelectron line was taken into account (Moulder et al. 1992). Survey and multiregion spectra were recorded for C1s, O1s, Ca2p and Mg2p photoelectron peaks. A depth profiling (up to 6 nm deep) was carried out by 4 keV Ar^+ bombardment. The at-depth scale of 3 nm min^{-1} is assumed to be equivalent to the sputter rate of Ta_2O_5 under the same sputter conditions. Differences in sputtering yield between the sample under study and Ta_2O_5 were not considered. Additionally, the microscopic surface features of dolomite crystals subjected to dissolution were observed using an optical microscope (Olympus BX60) equipped with a digital microphotography unit (Olympus DP10). Observations were performed both under transmitted and reflected (polarized) light.

3. RESULTS AND DISCUSSION

3.1. General features of dolomite dissolution

Dolomite dissolved on $\{10\bar{1}4\}$ cleavage surfaces by the formation and spreading of etch pits after the injection of highly undersaturated solutions into the fluid cell. Immediately after injection, the dolomite surface developed shallow (~0.3 nm height) rhombohedral pits at all values of pH tested (Fig. 1). This etch pit morphology is typically observed in other carbonates such as calcite during dissolution studies. Angles between steps delimiting etch pits were found to be ~77° and ~103°. The length ratio of the rhombus diagonals was found to be 0.92 ± 0.05, which differs from the value (~0.72) observed in the regular rhombohedral etch pits formed at all pH values on cleavage surfaces of single-cation $R\bar{3}c$ carbonates such as calcite and rhodochrosite ($MnCO_3$) (e.g. Pérez-Garrido et al, 2007). These

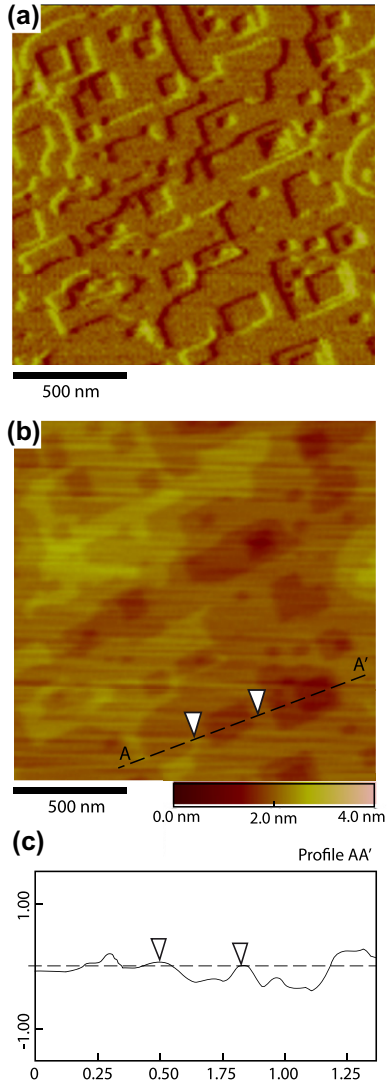

Fig. 1. AFM deflection (a) and topographic (b) images showing shallow, rhombohedral etch pits developed on $(10\bar{1}4)$ dolomite surface at pH 8. (c) Depth profile in section AA′ of the corresponding topographic image.

distorted rhombohedral etch pits were typically less than 200 nm wide before they coalesced and a one unit-cell layer was removed. Then new etch pits nucleated and spread, repeating the process (Fig. 2). The measured etch pit density was approximately constant from pH 3 to 10 and equal to 1.9×10^9 ($\pm 0.3 \times 10^9$) cm^{-2}, which is ca. 4 orders of magnitude higher than that observed by Lüttge et al. (2003) at acidic pH (~3) conditions using VSI. However, their study focused on deep etch pits (depth up to 2 μm), most probably nucleated at dislocations (MacInnis and Brantley, 1992). The observed average values of nucleation density were roughly one order of magnitude higher than those generally reported for calcite during dissolution in pure, deionized water (Teng 2004; Ruiz-Agudo et al., 2009). Shallow etch pits, such as those observed here during dolomite dissolution, nucleate at point defects (MacInnis and Brantley, 1992) as well as on defect-free surfaces, provided a sufficiently high undersaturation is reached (Teng 2004; Ruiz-Agudo et al., 2009). Examination under the optical microscope of Eugui dolomite single crystals subjected to dissolution (pH 3) showed the formation of scarce ($\sim 0.5 \times 10^4$ cm^{-2}) deep rhombohedral etch pits (Fig. 3). However, such deep etch pits were not present after flowing the acid solution for 30 min, but only visible after long term (>48 h) dissolution (pH 3) in a batch reactor. The measured low density of deep etch pits is consistent with the low density of dislocations in Eugui dolomite (Barber et al., 1981). The lower density of line defects in Eugui dolomite compared with calcite (ca. 10^6 cm^{-2}; Bisschop et al., 2006) may explain why deep etch pits are rarely observed here as well as in other AFM dissolution studies where Eugui dolomite crystals have been used (e.g., Ruiz-Agudo et al., 2011). In contrast, shallow etch pits were highly abundant and their nucleation and spreading appears to control the dissolution of dolomite, in the sense that under neutral to slightly alkaline pH conditions spreading and coalescence of shallow etch pits lead to the removal of dolomite surface layers before a stepwave generated at a deep etch pit (Lüttge et al., 2003) reaches a flat terrace and results in the removal of such layer.

Overall, dolomite dissolution shows characteristics of both Type I (Ca, Mn) and Type II (Fe, Mg) carbonates, according to the classification of Duckworth and Martin (2004). Flat surfaces with well-formed shallow etch pits such as those observed in our dissolution experiments are typically reported during dissolution of stoichiometric and well-ordered dolomite (Kaczmarek and Sibley, 2007). The observation of aspect ratios different from that of the perfect rhombohedron can be explained considering the lower symmetry of dolomite structure if compared with that of calcite. Dolomite crystallizes in the space group $R\bar{3}$, which differs from the $R\bar{3}c$ space group of calcite-type carbonates in the lack of the c-glide and diad axes (Reeder, 1983). Thus, the two obtuse steps are structurally different, as well as the acute steps (Fig. 4). Therefore, the etch pits may show non-regular rhombohedral geometries (Higgins and Hu, 2005). Due to the lower symmetry of dolomite if compared with calcite, four distinct step velocities are needed to define the spreading of the etch pits formed on dolomite cleavage surfaces (Higgins and Hu, 2005). However, differences found between etch pit spreading rates along $[\bar{4}41]$ and $[48\bar{1}]$ directions (Fig. 4) were within the experimental error of the measurements and thus the etch pit spreading rate values, v_{sum}, reported in this work refer on average to the rate of change in etch pit length along either $[\bar{4}41]$ or $[48\bar{1}]$ directions.

3.2. Dissolution kinetics: comparison with previous dissolution studies

Table 1 shows etch pit spreading rates (v_{sum}) as well as overall dissolution rates (R_{AFM}) calculated from AFM measurements according to Eqs. (1) and (2) for the different pH values tested. Ca and Mg concentrations in the outflow solutions are also shown in Table 1. Non-stoichiometric Ca/Mg ratios were found (i.e. Ca/Mg in the effluent solution was different from that of the solid). This observation will be further discussed in Section 3.3. To compare with

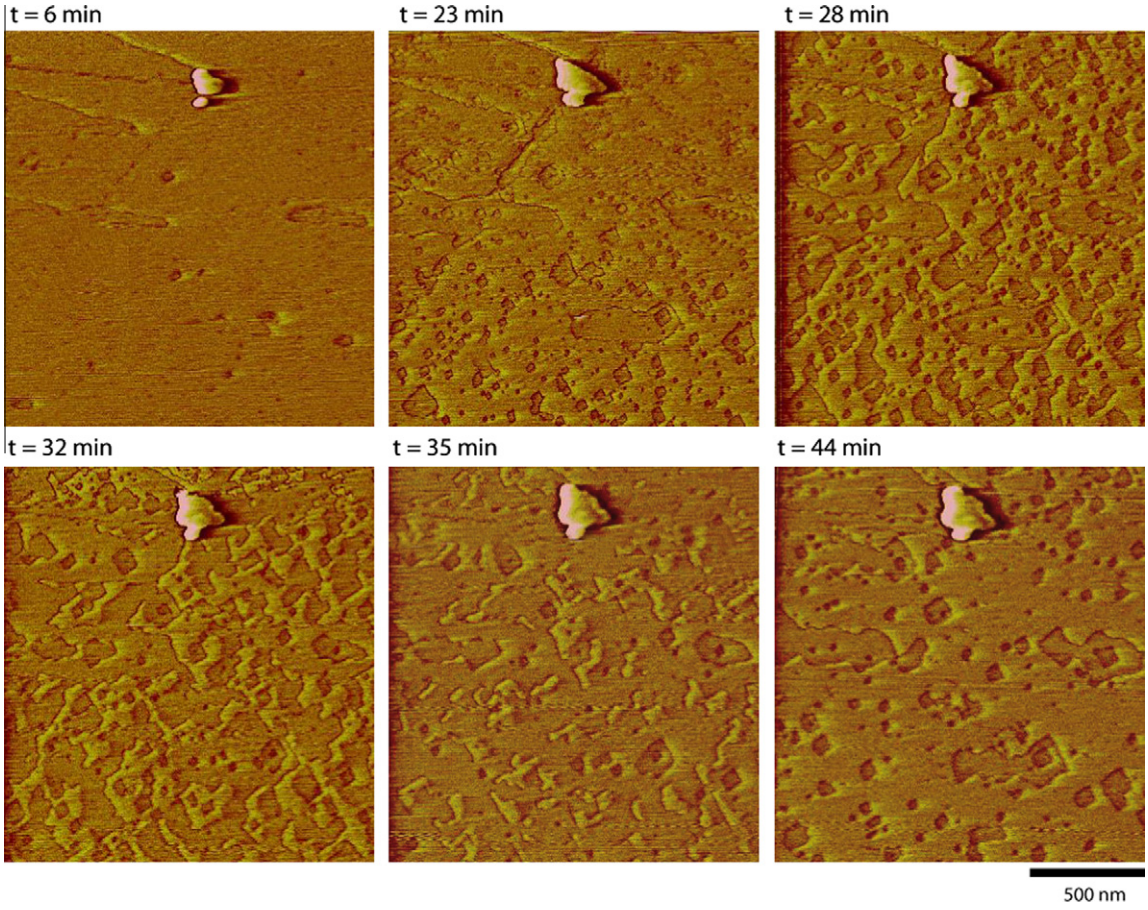

Fig. 2. AFM deflection images of a dolomite $(10\bar{1}4)$ surface exposed to deionized water for increasing periods of time. Average etch pit depth ~0.3 nm. Note the complete removal of an atomic layer after 35 min. and the nucleation and spreading of new shallow pits in the newly exposed layer after 44 min.

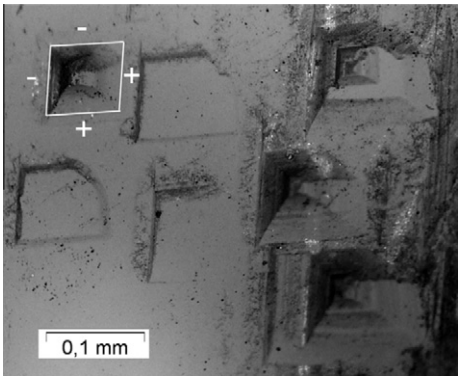

Fig. 3. Reflected light optical microscopy image of the dolomite $(10\bar{1}4)$ surface exposed to pH 3 solution for 48 h. Deep rhombohedral etch pits are observed (the acute − and obtuse + step edges are indicated).

R_{AFM}, macroscopic dissolution rates (R_{mac}) were calculated according to Eq. (3) using Ca concentrations in the outlet solutions (Table 1).

Fig. 5a summarizes some of the dolomite dissolution rate data published in the literature. In the present study, R_{AFM} of dolomite in deionized water (neutral pH) was found to be 7.4×10^{-13} ($\pm 1.6 \times 10^{-13}$) mol cm^{-2} s^{-1}. As can be seen in Fig. 5a, R_{AFM} values were nearly pH-independent in the range 5–10, while a slight increase in R_{AFM} values was observed at pH <5. The spreading rate showed a similar trend, with a tendency to increase for pH <5 (Fig. 5b).

To our knowledge only three previous studies have explored the kinetics of dolomite dissolution at the micro- and nanoscale. Ruiz-Agudo et al. (2011) carried out a systematic study of ion-specific effects on dolomite dissolution using in situ AFM, showing that different electrolytes modify dolomite dissolution kinetics, expressed as etch pit spreading rates, when compared with pure deionized water. Trends observed for the different electrolytes can be interpreted in terms of characteristic parameters of background ions, according to the way in which these electrolytes modify solute hydration and water structure dynamics. The etch pit spreading rate in deionized water (pH = 7) reported in that paper (0.09 ± 0.01 nm s^{-1}) is of the same order of magnitude than that found in the present study (0.058 ± 0.004 nm s^{-1}).

Hu et al. (2005) performed an in situ AFM study of the reactivity of cleavage surfaces of dolomite. However, they

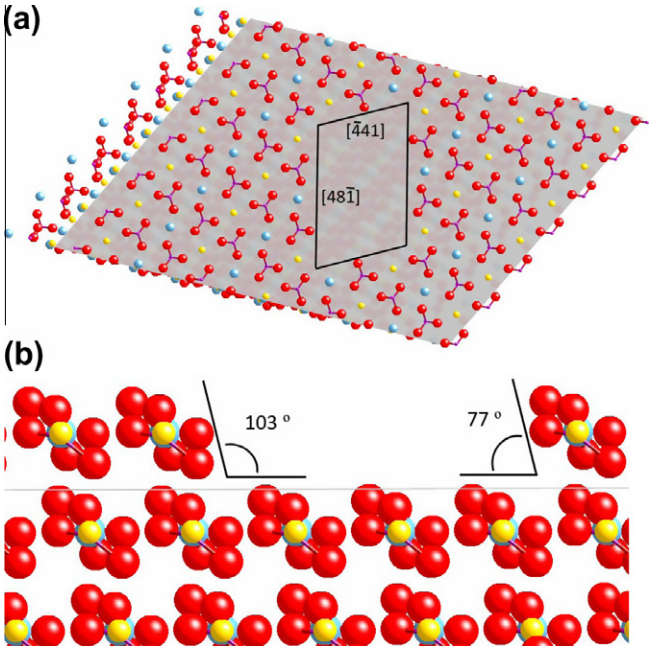

Fig. 4. (a) Normal view of the atomic arrangements in the cleavage plane of dolomite. (b) Sketch showing a cross-section of an etch pit, with the obtuse and acute step edges indicated. Color code: calcium (blue), magnesium (yellow), oxide (red), carbon (purple). (For interpretation of the references to color in this figure legend, the reader is referred to the web version of this article.)

Table 1
Etch pit spreading rates (v_{sum}), density of etch pits and overall dissolution rates (R_{AFM}) on dolomite cleavage surface as a function of pH, and concentrations of Ca^{2+} and Mg^{2+} in the outlet solutions and bulk dissolution rates (R_{mac}).

pH	v_{sum} (nm s^{-1})	Density (nm^{-2})	R_{AFM} (mol cm^{-2} s^{-1})	Ca^{2+} (mg/L)	Mg^{2+} (mg/L)	R_{mac} (mol cm^{-2} s^{-1})
3	0.0885 ± 0.0012	17.26	$16.80 \times 10^{-13} \pm 3.05 \times 10^{-13}$	2.455	0.018	3.420×10^{-9}
4	0.0615 ± 0.0017	17.61	$10.40 \times 10^{-13} \pm 1.95 \times 10^{-13}$	0.475	0.002	0.658×10^{-9}
5	0.0538 ± 0.0021	15.96	$9.21 \times 10^{-13} \pm 2.32 \times 10^{-13}$	0.170	0.000	0.237×10^{-9}
7	0.0581 ± 0.0036	22.51	$7.42 \times 10^{-13} \pm 1.62 \times 10^{-13}$	0.195	0.001	0.272×10^{-9}
8	0.0473 ± 0.0016	18.48	$9.28 \times 10^{-13} \pm 2.66 \times 10^{-13}$	0.145	0.000	0.202×10^{-9}
9	0.0441 ± 0.0014	22.04	$8.43 \times 10^{-13} \pm 2.19 \times 10^{-13}$	0.160	0.000	0.223×10^{-9}
10	0.0448 ± 0.0014	18.98	$8.81 \times 10^{-13} \pm 2.47 \times 10^{-13}$	0.010	0.000	0.014×10^{-9}

reported dissolution rates that cannot be directly compared with our data, as they worked under different conditions of undersaturation. They obtained values for v_{sum} and R_{AFM} of 3.4 nm h^{-1} (0.0012 nm s^{-1}) and 4.4×10^{-15} mol cm^{-2} s^{-1} (SI = −2.98) and 1.2 nm h^{-1} (0.0003 nm s^{-1}) and 1.5×10^{-15} mol cm^{-2} s^{-1} (SI = −1.17), at high pH (9) and 0.01 ionic strength (NaCl). The overall dolomite R_{AFM} dissolution rate measured at pH 3 in our study (calculated from etch pit density and spreading rate) is ca. 25 times lower than that reported at the same pH by Lüttge et al (2003) determined using VSI (4×10^{-11} mol cm^{-2} s^{-1}). This difference is not unexpected, as they measured dissolution rates in deep etch pits most probably originated at dislocations which represent regions of unusually high strain. The same authors calculated an absolute dissolution rate from surface retreat of 1.08×10^{-11} mol cm^{-2} s^{-1}. This value is closer to our measured value. Lüttge et al. (2003) compared their rate values with some published bulk measurements, such as those determined by Busenberg and Plummer (1982), Chou et al. (1989) and Gautelier et al. (1999), showing clear disagreements between them (bulk values were between one and two orders of magnitude higher than that obtained by VSI). Our macroscopic dissolutions rates (R_{mac}), show similar disagreement with Lüttge et al. (2003) VSI measurements, as well as with our own R_{AFM} values (Fig. 5a). As Lüttge et al. (2003) indicated, there are several reasons for the disagreement between bulk/macroscopic and nanoscale dissolution rates, including the normalization of rates by geometric areas in AFM or VSI experiments (instead of BET surface area) and the use of mineral powders (instead of the single crystals) in bulk experiments which are likely to expose highly reactive surfaces to the solution (see also Lüttge, 2005).

Pokrovsky et al. (1999) and Pokrovsky and Schott (2001) performed a comprehensive study of dolomite dissolution using mixed-flow reactors under different conditions of pH, ionic strength (NaCl) and undersaturation. These authors showed that below ca. pH 5.4, dissolution rates increase with decreasing pH whereas above this value they are pH independent in CO_2-poor solutions and decrease sharply with increasing pH in CO_2 enriched solutions. Under

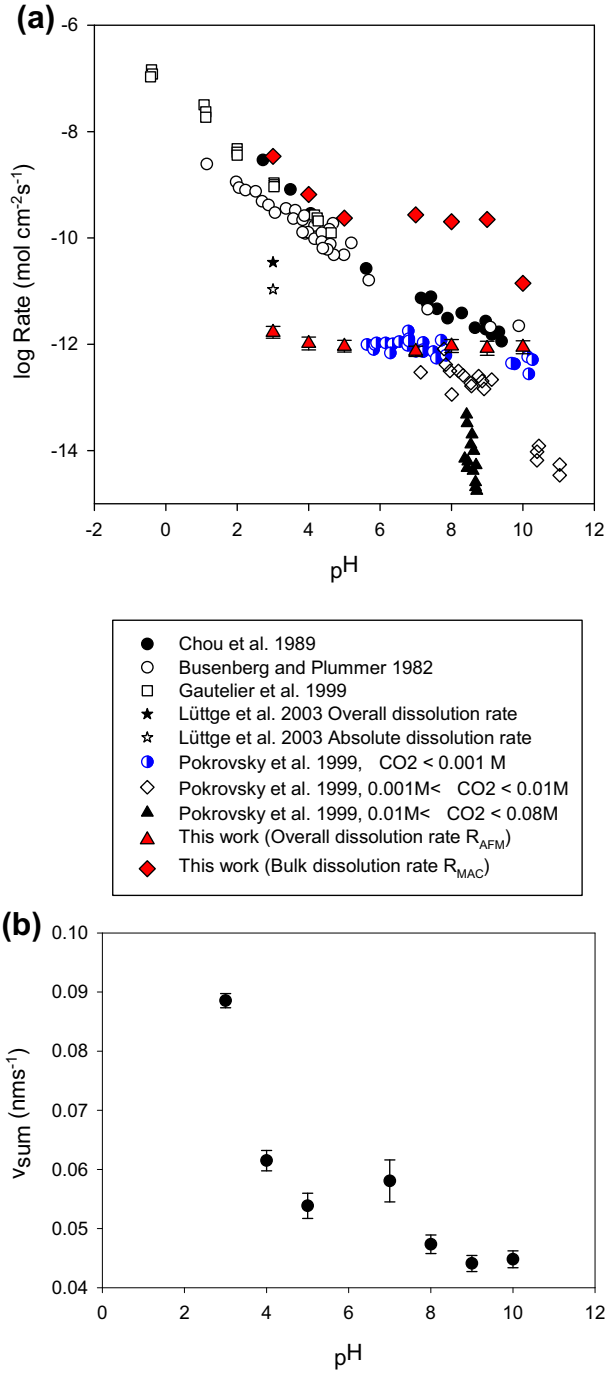

Fig. 5. (a) Comparison of AFM-derived (R_{AFM}) and macroscopic (R_{mac}) dolomite dissolution rates of the present work with those obtained from previous studies as a function of pH. (b) Etch pit spreading rates, v_{sum} (nm s^{-1}) on dolomite cleavage surfaces as a function of pH.

conditions of circumneutral to alkaline pH, low ionic strength (0.001) and low total dissolved carbonate (<0.001 M), they obtained values which are in remarkably good agreement with the R_{AFM} values reported in our study (see Fig. 5a).

Mineral dissolution rates can be determined by the kinetics of the surface reaction and/or the mass transport of the dissolved species from the crystal surface towards the bulk. The slowest of these processes will control the dissolution rate. It is generally accepted that, in contact with the mineral surface and separating it from the well-mixed, turbulent bulk solution, there is a "boundary layer" with a different composition from the bulk (Putnis et al. 2005). If the solution flow is slow, this boundary layer is thick and the time for the solutes to be transported through the layer is long and it can become the rate-limiting step in the dissolution process (Liu and Dreybrodt, 2001). Mass transport control on dissolution rates (reflected as a flow rate dependence on the velocity of step spreading) at acidic pH (<5.3) has been reported for other carbonates, such as calcite, up to flow rates of 119 mL h^{-1} in AFM experiments (Shiraki et al., 2000). Although the early macroscopic studies of dolomite dissolution (such as those published by Lund et al., 1973; Busenberg and Plummer, 1982 and Chou et al., 1989) suggested that the kinetics of the dissolution process is controlled by the surface reaction even at low pH (Orton and Unwin, 1993), later studies have shown that, as in the case of calcite, the kinetics of dolomite dissolution is diffusion controlled at acidic pH. Orton and Unwin (1993) provided evidence of mass-transport control on dolomite dissolution rates at low pH, even at fast flow rates (up to 0.125 cm^3 s^{-1} in their channel-flow set up). Liu and Dreybrodt (2001) showed that the presence of a diffusion boundary layer in contact with the mineral surface can significantly reduce dolomite dissolution rates. Furthermore, some of the studies reporting surface control on the kinetics of dolomite dissolution, such as those by Herman and White (1985) and Chou et al. (1989), were performed under conditions of high partial pressure of CO_2 ($P_{CO_2} > 1$ atm). However, it has been suggested that, for low partial pressures of CO_2, the mechanism controlling the kinetics of the reaction is different, and the rates become mass-transport controlled (Liu and Dreybrodt, 2001).

All in all, these observations give evidence of the relevance of mass transport and the diffusion boundary layer during the dissolution of dolomite at acidic pH and suggest that, under our experimental conditions and despite the fact that we used a relatively high flow rate of ca. 100 mL h^{-1} (a value double that used by Ruiz-Agudo et al., 2009, to fully ensure a reaction-controlled mechanism in the case of calcite dissolution), dolomite dissolution reaction is mass transport controlled at acidic pH.

3.3. Surface precipitates during the incongruent dissolution of dolomite

The dissolution of dolomite was accompanied by nucleation of a new phase on the dolomite surface (Fig. 6). This could well explain why Ca/Mg ratios in the effluent solution were different than that of the solid and much higher than 1, which itself suggests that the precipitating phase was a Mg-rich carbonate. The precipitation of this secondary phase was particularly evident at acidic pH (pH 3 and 4). The precipitated nuclei or three-dimensional islands rarely showed well-defined straight edges and reached a thickness of 2.2 ± 0.3 nm during the very early stages of their formation. The growth of this new phase occurred by lateral spreading

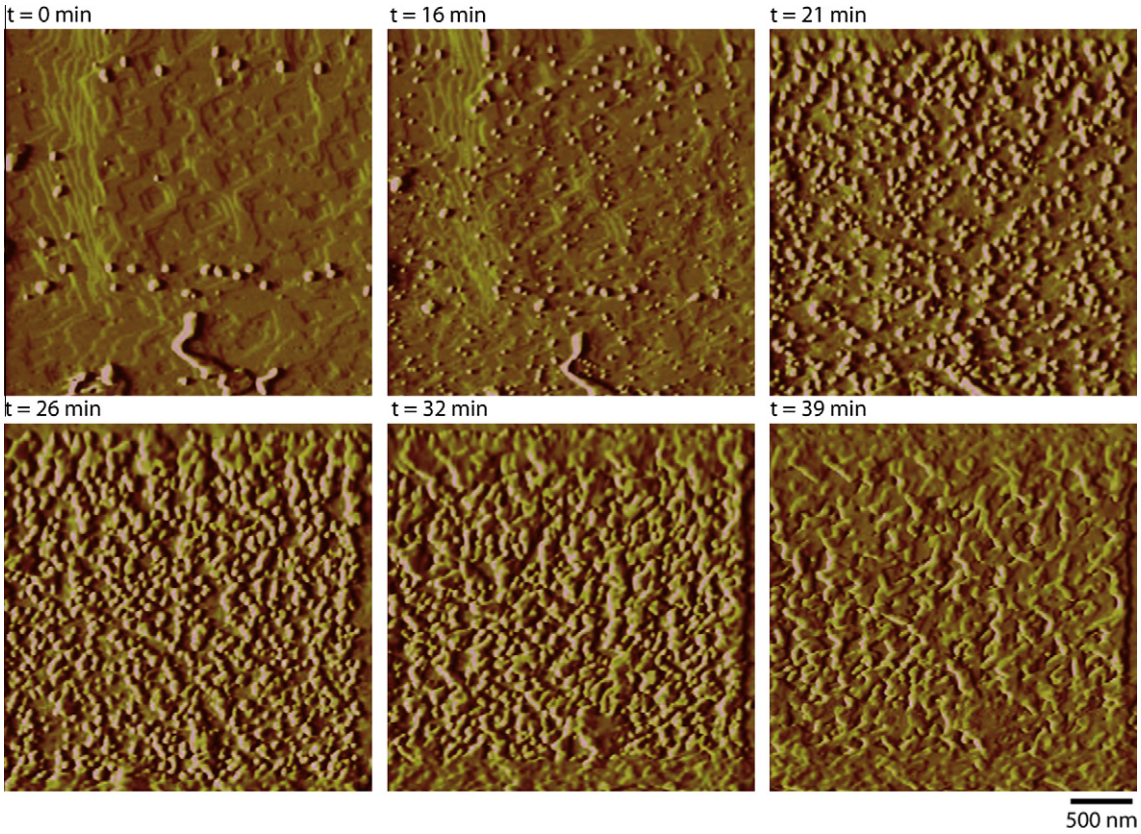

Fig. 6. Sequential AFM deflection images showing the formation of a Mg-rich phase on a dolomite cleavage surface at pH 3.

of the 3D islands leading eventually to their coalescence, without a significant increase in their height, that remained approximately constant during the whole growth process. Initially, the growth of this layer avoided the areas where etch pits previously existed, leading to the formation of a surface that reproduced the original dolomite surface.

One frequent source of divergence between dissolution rates determined in bulk and nanoscale experiments could arise from the fact that dissolution rates obtained from solution chemistry may be influenced by dolomite "incongruent" or "non-stoichimetric" dissolution. Several macroscopic dissolution studies have reported non-stoichiometric dissolution of dolomite, particularly in the first stages of the dissolution experiments (i.e., during the removal of up to two atomic layers of the solid surface). Busenberg and Plummer (1982) and later Pokrovsky and Schott (2001) and Zhang et al. (2007) suggested that preferential dissolution of the Ca-component and the formation of a Ca-depleted surface could explain the fact that Ca/Mg ratios in solution were initially higher than those of the bulk solid. The preferential release of the calcium component to the solution was explained on the basis of the much lower hydration energy of Ca^{2+} if compared with Mg^{2+} and thus its lower stability at the dolomite/water interface (Pokrovsky and Schott, 2001). A similar mechanism has been proposed to explain the non-stoichiometric dissolution behavior of other minerals, such as wollastonite (CaSiO3), although in this case the possibility of a precipitation event was not ruled out (Green and Lüttge, 2006). However, from our in situ, nanoscale observations of the reacting surface we found no experimental evidence that supports the hypothesis of a preferential release of calcium. Moreover, our AFM results clearly indicate that this "incongruent" behavior (non-stoichiometric dissolution) is the result of a dissolution-precipitation process, as reflected in the height profiles shown in Fig. 7, where the newly-formed topographic features are clearly the result of a growth process.

According to our observations, dolomite dissolution occurs at step edges parallel to $\langle\bar{4}41\rangle$, and dissolution at such step edges is a stoichiometric process, i.e. equal amounts of Ca^{2+} and Mg^{2+} are present along such steps and thus are equally released to the solution as the steps spread. Hu et al. (2005) indicated that a possible pathway for the generation of Mg-enriched surfaces during dolomite dissolution could be the preferential detachment of calcium ions from terraces, generating point defects at these flat surfaces. Etch pits would immediately nucleate at these defects, and in fact this could possibly explain the higher etch pit density observed in the case of dolomite compared to calcite. However, this would just be a transient stage, and the immediate spreading of these newly formed etch pits would lead to stoichiometric dissolution.

3.4. Characterization of surface precipitates

The scarcity of well formed peaks in the XRD pattern of dolomite crystals treated with HCl aqueous solutions (pH 3) obtained by the grazing incident angle method

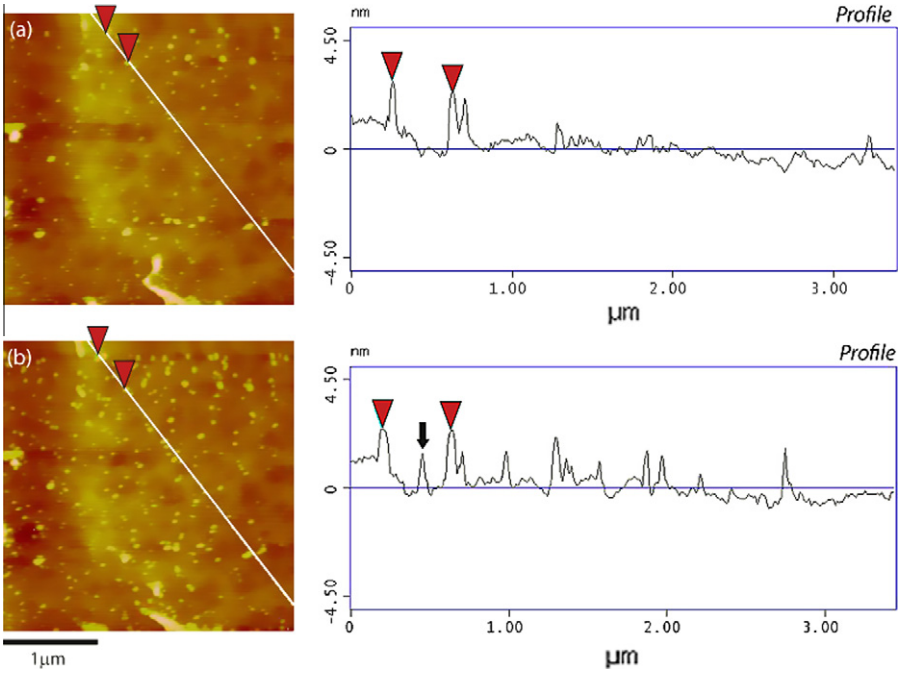

Fig. 7. Sequential AFM height images showing the formation of surface precipitates. The depth profiles show the upward growth (i.e., height increase indicated with black arrow) of such a newly formed phase. The time lapse between images is 104 s.

(GIAXRD) precludes the unambiguous identification of the Mg-rich phase formed. However, the peaks present in the XRD pattern shown in Fig. 8 match those of nesquehonite. Unfortunately, this could not be fully confirmed by XPS (Table 2), possibly due to the low percentage of the dolomite surface covered by this secondary phase. The XPS results nevertheless confirm the purity and stoichiometry of the dolomite used in our experiments.

It is plausible that the detachment, hydration (Hu et al. 2005) and/or diffusion to the bulk of the magnesium ions adsorbed at the dolomite surface is sufficiently slow to result in a magnesium enrichment of the dolomite surface or the solution layer immediately in contact with the surface. This is supported by the lower rate of desorption and smaller diffusion coefficient (Guàrdia et al., 1999), as well as the higher residence time at the mineral/solution

Table 2
Ca/Mg atomic ratios measured by X-Ray Photoelectron Spectroscopy (XPS) in raw and partially dissolved samples as a function of depth.

Depth	Dolomite control	Dolomite HCl
Surface	0.924	0.935
3 nm	0.999	0.996
6 nm	1.058	1.014

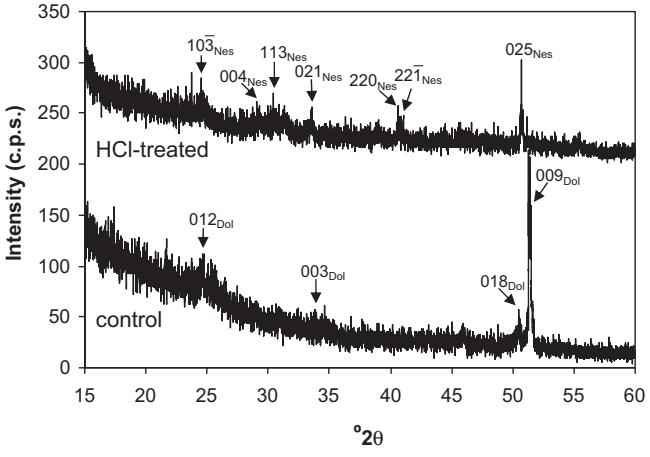

Fig. 8. Grazing angle X-ray diffraction patterns of dolomite ($10\bar{1}4$) surface before dissolution (control) and following dissolution at pH 3 (HCl-treated). Bragg peaks of dolomite (hkl_{dol}) and nesquehonite (hkl_{nes}) are indicated.

interface (Kerisit and Parker, 2004) of magnesium if compared with calcium. All in all, any of these effects could lead to the development of steep concentration gradients close to the surface of the mineral, as observed by Putnis et al. (2005) during mineral dissolution/replacement reactions using real time phase-shift interferometry. The authors reported that dissolution of a parent phase (KBr) in a saturated KCl solution results in an interfacial fluid layer that is supersaturated with respect to a different solid composition (K(Br, Cl)), while the bulk solution is undersaturated with respect to such a phase. As a result, a tightly coupled dissolution/precipitation reaction at the mineral-fluid interface occurs. As stated above, development of a concentration gradient and magnesium enrichment at the dolomite/solution interface is likely to occur, resulting in the fluid being locally supersaturated with respect to nesquehonite.

In our system, supersaturation with respect to nesquehonite could have been locally reached following the formation of a similar interfacial fluid layer with composition different from the bulk, leading to the eventual formation of such a surface precipitate. Supersaturation with respect to other phase/s could also be reached at the interface, but the precipitation of this/these other phase/s may be kinetically unfavorable for unknown reasons. If dolomite dissolves and instantaneously equilibrates with the bulk solution, thermodynamic calculations performed using PHREEQC (Table 3) indicate that the bulk solution is undersaturated with respect to all possible phases except magnesite ($MgCO_3$). Due to the short contact time between the solid and the fluid in our flow-through set up, equilibrium with respect to dolomite is not expected to be reached and this is just considered as a reference or threshold case for our experiments. It is well known that, despite being the stable Mg-carbonate form, the precipitation of magnesite under normal P–T conditions of the Earth surface is virtually impossible (Hänchen et al., 2008). Thus the formation of this phase may be disregarded in our experiments. Mg-carbonate precipitation is strongly kinetically controlled, and it has been suggested that the highly hydrated character of the Mg^{2+} ion in aqueous solution is responsible for the difficulty in precipitating anhydrous Mg-bearing carbonates (magnesite and dolomite) (Sayles and Fyfe, 1973). Most commonly, nesquehonite ($MgCO_3{\cdot}3H_2O$), hydromagnesite ($(MgCO_3)_4{\cdot}Mg(OH)_2{\cdot}4H_2O$) and landsfordite ($MgCO_3{\cdot}5H_2O$) are formed in laboratory studies under ambient conditions (see for example Hänchen et al., 2008 and references therein).

Thus, our experimental results suggest that this interface-coupled dissolution-precipitation reaction (Putnis and Putnis, 2007) is controlled by the fluid composition in a boundary layer at the interface with the solid dolomite substrate. This boundary layer will have a different composition to the fluid in the bulk because, on dissolution of the substrate, it becomes supersaturated with respect to a new phase which then precipitates simultaneously, or is coupled to further dolomite dissolution. Therefore, according to our observations we suggest that the interaction of dolomite with aqueous solutions is a two-step process: (i) congruent dissolution of the primary mineral by formation and spreading of shallow (i.e. 0.3 nm deep) etch pits and (ii) subsequent precipitation of a Mg-rich phase. The fact that growth initially stops at the edges of dolomite etch pits, reproducing the topography of the parent solid (i.e. the template effect, Astilleros et al., 2003), indicates a crystallographic mismatch between the substrate and the overgrowth.

Note that it has been reported that the so-called "incongruent" dissolution is a transient stage, typically observed during the early stages of dolomite dissolution (Busenberg and Plummer, 1982). Over time, the solution Ca/Mg ratio approaches unity. This implies that the newly formed Mg-rich surface layer we have observed should redissolve as dissolution progresses. This is actually what we have seen under the AFM (Fig. 9), where the newly formed precipitate continuously dissolves and reprecipitates during the course of the experiment. This is not unexpected as the steep

Table 3
Solution speciation and saturation state with respect to relevant carbonate phases calculated using PHREEQC (database: sit.dat) for a solution of initial pH 3 in equilibrium with dolomite.

pH	8.191			
Solution speciation				
C(4)			1.04E−03	M
	Specie	***Molality***	***Activity***	
	HCO_3-	1.00E−03	9.43E−04	
	CO_2	1.36E−05	1.36E−05	
	CO_3^{-2}	8.72E−06	6.85E−06	
	$Ca(HCO_3)+$	5.06E−06	4.76E−06	
	$CaCO_3$	4.56E−06	4.56E−06	
	$Mg(HCO_3)+$	4.42E−06	4.16E−06	
	$Mg(CO_3)$	2.64E−06	2.64E−06	
Ca			5.20E−04	M
	Specie	***Molality***	***Activity***	
	Ca+2	5.11E−04	4.01E−04	
	$Ca(HCO_3)+$	5.06E−06	4.76E−06	
	$CaCO_3$	4.56E−06	4.56E−06	
	CaCl+	2.13E−07	2.01E−07	
	Ca(OH)+	1.10E−08	1.03E−08	
	$CaCl_2$	8.74E−11	8.74E−11	
Mg			5.20E−04	M
	Specie	***Molality***	***Activity***	
	Mg+2	5.12E−04	4.03E−04	
	$Mg(HCO_3)+$	4.42E−06	4.16E−06	
	$Mg(CO_3)$	2.64E−06	2.64E−06	
	MgCl+	9.34E−07	8.79E−07	
	Mg(OH)+	1.39E−07	1.31E−07	
Solid phases				
	Phase	***Saturation index***	**log K_{sp}**	
	Aragonite	−0.25	−8.31	
	Calcite	−0.08	−8.48	
	Dolomite	0	−17.12	
	Lansfordite	−3.52	−5.04	
	Magnesita	0.35	−8.91	
	$Mg5(CO_3)4(OH)\cdot4H_2O$(s)	−10.94	−10.31	
	Nesquehonite	−3.23	−5.33	
	Vaterite	−0.66	−7.9	

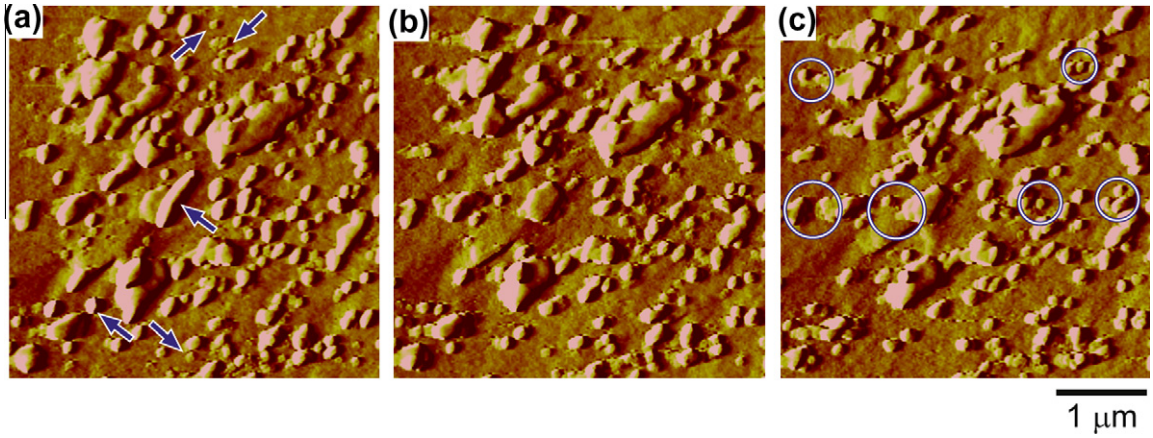

Fig. 9. Sequential AFM height images showing the (a) dissolution of some of the precipitates covering the surface (blue arrows) when compared with (b) and (c) the growing and nucleation of precipitates (circles). The time lapse between images is 101 s. The pH of the solution is 3. (For interpretation of the references to colour in this figure legend, the reader is referred to the web version of this article.)

concentration gradient existing at the dolomite–solution boundary layer will be changed due to the precipitation of this phase and the supply of fresh solution, thus promoting the dissolution of this phase. In fact, PHREEQC thermodynamic calculations show that the bulk solution is undersaturated with respect to this Mg-rich carbonate phase (most probably nesquehonite, as indicated by XRD analysis).

We suggest that a balance between Ca and Mg fluxes in the output may be eventually reached as reflected in the Ca/Mg ratio ≈ 1 measured in the outflow in bulk experiments at long times (Busenberg and Plummer, 1982; Zhang et al., 2007). This implies that the formation of such a Mg-rich layer will not be necessarily limited to the very early stages of dolomite dissolution, only affecting a few (one or two) atomic layers as suggested by Busenberg and Plummer (1982). In fact, it is difficult to envision a mechanistic scenario explaining why either just the first layer or the first two atomic layers will be the only ones involved in the so-called "non-stoichimetric" or "incongruent" dissolution of dolomite as suggested by Busenberg and Plummer (1982) and Pokrovsky and Schott (2001). In summary, this discussion highlights the importance of using techniques such as AFM that allow in situ, direct nanoscale observations of the mineral surface during dissolution to ascertain the mechanism and kinetics of mineral dissolution.

4. CONCLUSIONS

The results of this study suggest that the overall dolomite dissolution rate under circumneutral to alkaline conditions is controlled by the removal of dolomite layers by spreading and coalescence of shallow etch pits rather than by step retreat from deep pits nucleated at high energy points (dislocations). Our results also suggest that dolomite dissolution rates obtained from measurements of the solution chemistry could be misestimated both due to an underestimation of reactive surface area, and as a consequence of the precipitation of a secondary phase, particularly at acidic pHs. This process is a coupled dissolution-precipitation reaction, ultimately controlled by the hydrodynamic conditions of the system and the formation of a boundary layer where supersaturation with respect to a secondary phase is reached. In situ, direct observations of the reacting mineral surface become critical in systems where "incongruent" dissolution is assumed, in order to unambiguously ascertain the mechanism and kinetics of mineral dissolution. For this reason, in situ AFM is a valuable tool in mineral dissolution studies as it allows quantification of the kinetics of the process from the measurement of etch pit densities and spreading rates, which are unaffected by the formation of any secondary precipitates. AFM in turn helps identifying the formation of secondary precipitates during dissolution, thus yielding critical mechanistic information.

ACKNOWLEDGMENTS

This work was carried out within the EU Initial Training Network Delta-Min (Mechanisms of Mineral Replacement Reactions) Grant PITN-GA-2008-215360. Experimental facilities in Münster are supported by the Deutsche Forschungsgemeinschaft (DFG). M. Urosevic acknowledges the Spanish Ministry of Innovation, Science and Technology for financial support through a FPU Grant (AP2006-060). Additional funding was provided by the research group NRM-179 (Junta de Andalucía, Spain) and the Spanish government under Grant MAT2009-11332. We thank M. V. Martinez de Yuso Garcia for her help during XPS analyses and Veronika Rapelius for the ICP-OES analyses.

REFERENCES

Arvidson R. S., Collier M., Davis K. J., Vinson M. D., Amonette J. E. and Luttge A. (2006) Magnesium inhibition of calcite dissolution kinetics. *Geochim. Cosmochim. Acta* **70**, 583–594.

Astilleros J. M., Pina C. M., Fernández-Díaz L. and Putnis A. (2003) Metastable phenomena on calcite {10-14} surfaces growing from $Sr^{2+} - Ca^{2+} - CO_3^{2-}$ aqueous solutions. *Chem. Geol.* **193**, 93–107.

Barber D. J., Heard H. C. and Wenk H. R. (1981) Deformation of dolomite single crystals from 20–800 °C. *Phys. Chem. Mineral.* **7**, 271–286.

Bell F. G. (1993) Durability of carbonate rock as building stone with comments on its preservation. *Environ. Geol.* **21**(4), 187–200.

Bisschop J., Dysthe D. K., Putnis C. V. and Jamtveit B. (2006) In situ AFM study of the dissolution and recrystallization behaviour of polished and stressed calcite surfaces. *Geochim. Cosmochim. Acta* **70**, 1728–1738.

Busenberg E. and Plummer L. N. (1982) The kinetics of dissolution of dolomite in CO_2 H_2O systems at 1.5 to 65 degrees C and O to 1 atm pco_2. *Am. J. Sci.* **282**(1), 45–78.

Cardell Fernández C., Vleugels G., Torfs K. and Van Grieken R. (2002) The process dominating Ca dissolution of limestone when exposed to ambient atmospheric conditions as determined by comparing dissolution models. *Environ. Geol.* **43**, 160–171.

Charola A. E. and Ware R. (2002) Acid deposition and the deterioration of stone: a brief review of a broad topic. In *Natural Stone, Weathering Phenomena, Conservation Strategies, Case Studies* (eds. S. Siegesmund, R. Weiss and A. Vollbrecht). Geol. Soc. Lond. Spec. Publ, pp. 393–406.

Chou L., Garrels R. M. and Wollast R. (1989) Comparative study of the kinetics and mechanisms of dissolution of carbonate minerals. *Chem. Geol.* **78**(3–4), 269–282.

Duckworth O. W. and Martin S. T. (2004) Dissolution rates and pit morphologies of rhombohedral carbonate minerals. *Am. Mineral.* **89**(4), 554–563.

Fenter P., Zhanga Z., Parka C., Sturchio N. C., Hu X. M. and Higgins S. R. (2007) Structure and reactivity of the dolomite (1 0 4)–water interface. New insights into the dolomite problem. *Geochim. Cosmochim. Acta* **71**(3), 566–579.

Ford D. C. and Williams P. (2007) *Karst Hydrogeology and Geomorphology*. Wiley-Blackwell, pp. 576.

Gautelier M., Oelkers E. H. and Schott J. (1999) An experimental study of dolomite dissolution rates as a function of pH from −0.5 to 5 and temperature from 25 to 80 °C. *Chem. Geol.* **157**(1–2), 13–26.

Gautelier M., Schott J. and Oelkers E. H. (2007) An experimental study of dolomite dissolution rates at 80 °C as a function of chemical affinity and solution composition. *Chem. Geol.* **242**(3–4), 509–517.

Guàrdia E., Sesé G., Padró J. A. and Kalko S. G. (1999) Molecular dynamics simulation of Mg^{2+} and Ca^{2+} ions in water. *J. Solution Chem.* **28**(10), 1113–1126.

Green E. and Lüttge A. (2006) Incongruent dissolution of wollastonite measured with vertical scanning interferometry. *Am. Mineral.* **91**(2–3), 430–434.

Hänchen M., Prigiobbe V., Baciocchi R. and Mazzotti M. (2008) Precipitation in the Mg-carbonate system–effects of temperature and CO_2 pressure. *Chem. Eng. Sci.* **63**, 1012–1028.

Herman J. S. and White W. B. (1985) Dissolution kinetics of dolomite: effects of lithology and fluid flow velocity. *Geochim. Cosmochim. Acta* **49**(10), 2017–2026.

Higgins S. R. and Hu X. (2005) Self-limiting growth on dolomite: experimental observations with in situ atomic force microscopy. *Geochim. Cosmochim. Acta* **69**(8), 2085–2094.

Higgins S. R., Hu X. and Fenter P. (2007) Quantitative lateral force microscopy study of the dolomite (1 0 4)–water interface. *Langmuir* **23**(17), 8909–8915.

Hoke G. D. and Turcotte D. L. (2004) The weathering of stones due to dissolution. *Environ. Geol.* **46**(3), 305–310.

Hu X., Grossie D. A. and Higgins S. R. (2005) Growth and dissolution kinetics at the dolomite–water interface. An in-situ scanning probe microscopy study. *Am. Mineral.* **90**, 963–968.

Kaczmarek S. E. and Sibley D. F. (2007) A comparison of nanometer-scale growth and dissolution features on natural and synthetic dolomite crystals: implications for the origin of dolomite. *J. Sed. Res.* **77**(5), 424–432.

Kerisit S. and Parker S. C. (2004) Free energy of adsorption of water and metal ions on the 1 0 4 calcite surface. *J. Am. Chem. Soc.* **126**, 10152–10162.

Lippman F. (1973) *Sedimentary Carbonate Minerals*. Springer-Verlag, Berlin.

Liu Z. and Dreybrodt V. (2001) Kinetics and rate-limiting mechanisms of dolomite dissolution at various CO_2 partial pressures. *Sci. China B* **44**(5), 500–509.

Lund K., Fogler H. S. and McCune C. C. (1973) Acidization–I. The dissolution of dolomite in hydrochloric acid. *Chem. Eng. Sci.* **28**(3), 691–700.

Lüttge A. (2005) Etch pit coalescence, surface area, and overall mineral dissolution rates. *Am. Mineral.* **90**, 1776–1783.

Lüttge A., Winkler U. and Lasaga A. C. (2003) Interferometric study of the dolomite dissolution: a new conceptual model for mineral dissolution. *Geochim. Cosmochim. Acta* **67**(6), 1099–1116.

Mann S. (2001) *Biomineralization: Principles and Concepts in Bioinorganic Materials Chemistry*. Oxford University Press, Oxford, pp. 216.

MacInnis I. N. and Brantley S. L. (1992) The role of dislocations and surface morphology in calcite dissolution. *Geochim. Cosmochim. Acta* **56**, 1113–1126.

Millero F. J. (2007) The marine inorganic carbon cycle. *Chem. Rev.* **107**(2), 308–341.

Morse J. W. and Arvidson R. S. (2002) The dissolution kinetics of major sedimentary carbonate minerals. *Earth Sci. Rev.* **58**(1–2), 51–84.

Morse J. W., Arvidson R. S. and Lüttge A. (2007) Calcium carbonate formation and dissolution. *Chem. Rev.* **107**(2), 342–381.

Moulder J. F., Stickle W. F., Sobol P. E. and Bomben K. D. (1992) *Handbook of X-ray Photoelectron Spectroscopy* (ed. J. Chastain). Perkin–Elmer Corporation, Minneapolis, pp. 393–406.

Oelkers E. H. and Schott J. (2005) Geochemical aspects of CO_2 sequestration. *Chem. Geol.* **217**(3–4), 183–186.

Orton R. and Unwin P. R. (1993) Dolomite dissolution kinetics at low pH: a channel-flow study. *J. Chem. Soc. Faraday Trans.* **89**(21), 3947–3954.

Paquette J. and Reeder R. J. (1995) Relationship between surface structure, growth mechanism, and trace element incorporation in calcite. *Geochim. Cosmochim. Acta* **59**, 735–749.

Pérez-Garrido C., Fernández-Díaz L., Pina C. M. and Prieto M. (2007) In situ AFM observations of the interaction between calcite (10–14) surfaces and Cd-bearing aqueous solutions. *Surf. Sci.* **601**, 5499–5509.

Pokrovsky O. S., Golubev S. V. and Schott J. (2005) Dissolution kinetics of calcite, dolomite and magnesite at 25 °C and 0 to 50 atm pCO2. *Chem. Geol.* **217**(3–4), 239–255.

Pokrovsky O. S. and Schott J. (2001) Kinetics and mechanism of dolomite dissolution in neutral to alkaline solutions revisited. *Am. J. Sci.* **301**(7), 597–626.

Pokrovsky O. S., Schott J. and Thomas F. (1999) Dolomite surface speciation and reactivity in aquatic systems. *Geochim. Cosmochim. Acta* **63**(19–20), 3133–3143.

Putnis A. and Putnis C. V. (2007) The mechanism of reequilibration of solids in the presence of a fluid phase. *J. Solid State Chem.* **180**, 1783–1786.

Putnis C. V., Tsukamoto K. and Nishimura Y. (2005) Direct observations of pseudomorphism: compositional and textural evolution at a fluid-solid interface. *Am. Min.* **90**, 1909–1912.

Reeder R.J. (1983) Crystal chemistry of the rhombohedral carbonates. In *Carbonates: Mineralogy and Chemistry* (ed. R. J. Reeder); *Rev. Mineral.* **11**, 1–47. Mineralogical Society of America.

Ruiz-Agudo E., Kowacz M., Putnis C. V. and Putnis A. (2010) The role of background electrolytes on the kinetics and mechanism of calcite dissolution. *Geochim. Cosmochim. Acta* **74**(4), 1256–1267.

Ruiz-Agudo E., Putnis C. V., Jiménez-López C. and Rodriguez-Navarro C. (2009) An atomic force microscopy study of calcite dissolution in saline solutions: The role of magnesium ions. *Geochim. Cosmochim. Acta* **73**(11), 3201–3217.

Ruiz-Agudo E., Urosevic M., Putnis C. V., Rodríguez-Navarro C., Cardell C. and Putnis A. (2011) Ion-specific effects on the kinetics of mineral dissolution. *Chem. Geol.* **281**(3–4), 364–371.

Sayles F. L. and Fyfe W. S. (1973) The crystallization of magnesite from aqueous solution. *Geochim. Cosmochim. Acta* **37**, 87–99.

Shiraki R., Rock P. A. and Casey W. H. (2000) Dissolution kinetics of calcite in 0.1 M NaCl solution at room temperature: An atomic force microscopic (AFM) study. *Aq. Geochem.* **6**, 87–108.

Teng H. H. (2004) Control by saturation state on etch pit formation during calcite dissolution. *Geochim. Cosmochim. Acta* **68**, 253–262.

Zhang R., Hu S., Zhang X. and Yu W. (2007) Dissolution kinetics of dolomite in water at elevated temperatures. *Aq. Geochem.* **13**(4), 309–338.

Associate editor: Dimitri A. Sverjensky